Continental Shelf Research 191 (2019) 104005

Contents lists available at ScienceDirect

Continental Shelf Research

journal homepage: http://www.elsevier.com/locate/csr

Research papers

Characterizing the influence of Atlantic water intrusion on water mass formation and phytoplankton distribution in Kongsfjorden, Svalbard

Courtney M. Payne [a,b], Collin S. Roesler [a,*]

[a] Department of Earth and Oceanographic Science, Bowdoin College, Brunswick, ME, 04011, USA
[b] Currently, Department of Earth System Science, Stanford University, Stanford, CA, 94305, USA

ARTICLE INFO

Keywords:
Arctic fjord
Atlantic water
Phytoplankton
Sea ice loss
Tidewater glaciers
Sediment plumes

ABSTRACT

Warm water intrusion into Arctic fjords is increasingly affecting polar ecosystems. This study investigated how Atlantic water intrusion and tidewater glacial melting impacted water mass formation and phytoplankton distribution in Kongsfjorden, Svalbard. Field data were collected over a 2-week period during the height of the melt season in August 2014 and were contextualized within an 18-year regional MODIS satellite record. Since 1998, intruding waters have warmed by 4–5.5 °C, which has prevented sea ice formation and changed the characteristics of fjord bottom waters. Modeled light fields suggest that suspended sediment in this glacial meltwater has reduced the euphotic zone close to the ice face, contributing to lower phytoplankton concentrations in both persistent and intermittently sediment-laden meltwater plumes. However, measurements collected close to terrestrially terminating glaciers indicate that turbidity is significantly lower in the meltwater plumes, resulting in deep euphotic zones and high phytoplankton concentrations. The results of this study support a three-part conceptual model of the effects of warm-water intrusion on water mass formation and primary production within 10 km of tidewater glaciers. Initially, warm water intrusion reduces sea ice coverage, which increases the euphotic depth and increases phytoplankton biomass. Warm water intrusions may also result in increased melting of tidewater glaciers, enhanced sediment release, reduction in euphotic depth and reduction in phytoplankton biomass. Ultimately, as tidewater glaciers retreat and become terrestrially terminating, the sediment load decreases, the euphotic zone again increases, and phytoplankton biomass increases.

1. Introduction

The Arctic has changed rapidly during the 21st century. Air temperature has risen disproportionately in the region over the past 50 years (Bekryaev et al., 2010; Overland et al., 2017; Pithan and Mauritsen, 2014; Screen and Simmonds, 2010) and is projected to increase by three times the global rate by 2100 (Kattsov et al., 2005). Warm Atlantic water has increased its inflow into the Arctic Ocean since the early 2000s, causing an unprecedented increase in sea surface temperature (SST) (Nilsen et al., 2016; Osborne et al., 2018; Pavlov et al., 2013; Polyakov et al., 2012, 2011; 2005; Spielhagen et al., 2011; Walczowski and Piechura, 2007). In ecosystems that have historically balanced at temperatures close to freezing, ocean temperature increases of just a few degrees Celsius can affect sea ice conditions, which can have dramatic consequences in terms of distribution, phenology, and taxonomy of primary production (Arrigo et al., 2008; Arrigo and Dijken, 2015; Li et al., 2009; Neukermans et al., 2018). Warm Atlantic water intrusion into Arctic-type fjords may make conditions inhospitable for certain Arctic species, limiting their ranges significantly (Hegseth and Sundfjord, 2008; Wassmann, 2011) while allowing organisms formerly confined to lower latitudes to replace endemic species (Grebmeier, 2012; Post et al., 2009).

These increasing Arctic temperatures have been associated with rapid retreat of tidewater glaciers (Holland et al., 2008; Luckman et al., 2015; Motyka et al., 2013; Rignot et al., 2010; Straneo and Heimbach, 2013; Truffer and Motyka, 2016), which are susceptible to both warming air and ocean temperatures. While land-terminating glaciers ablate only through atmospheric melting at the glacier surface, marine-terminating glaciers can also lose mass as a result of convection at the ocean-glacier interface and submarine melting, destabilization, and calving (Jenkins, 2011; Luckman et al., 2015; Straneo and Cenedese, 2015; Straneo and Heimbach, 2013). Following the sudden increase in subsurface ocean water temperature along the west coast of Greenland in 1997, Sermek Kujalleq (also known by its Danish

* Corresponding author.
E-mail addresses: cmpayne@stanford.edu (C.M. Payne), croesler@bowdoin.edu (C.S. Roesler).

https://doi.org/10.1016/j.csr.2019.104005
Received 19 February 2019; Received in revised form 23 October 2019; Accepted 27 October 2019
Available online 5 November 2019

name, Jakobshavn Isbrae) in Disko Bay experienced a doubling in glacial velocity, becoming the most rapidly retreating glacier in the world. Holland et al. (2008) attribute this increase to the destabilization and melting of the floating ice tongue in front of the glacier. Increased summer melting led to the retreat of the terminus of the glacier to a 1300 m deep portion of the basin by 2013, exposing an even greater melting face to warming ocean waters and further increasing the summer velocity (Joughin et al., 2014). Similarly, at the temperate tidewater LeConte glacier in Alaska, a warm (7.2 °C) layer of water extending from 130 m depth to the fjord floor caused increased submarine melting of the glacier and greatly accelerated glacial retreat in 2000 (Motyka et al., 2013). While warming waters have been correlated with increased glacial melting and retreat, the mechanisms underpinning this relationship are still poorly understood, and atmospheric forcing, altered fjord-scale circulation (Slater et al., 2018), or other forcings could instead drive increases in subglacial discharge.

Terrestrially-terminating glaciers often deposit sediment in lakes, moraines, or braided rivers, so when glacial meltwater reaches the ocean, there is little suspended glacial sediment. In contrast, tidewater glaciers basally transport sediment-rich meltwater to their marine terminus, where the meltwater generally forms sediment plumes that can increase surface marine turbidity if the grounding zone is sufficiently shallow. At the tidewater McBride Glacier in Alaska, rapid retreat (0.25 km yr^{-1}, 1984-86) led to the deposition of 6.6×10^6 m^3 of sediment over a two-year period, with sediment accumulation rates as high as 13 m yr^{-1} at a distance of 300 m from the glacier (Cowan and Powell, 1991). Approximately 2/3 of the total volume of sediment was emitted by meltwater plumes originating at the base of the tidewater glacier, and was subsequently deposited by suspension settling (Cowan and Powell, 1991). Despite sediment flocculation close to the glacier, fine particles stay suspended even several kilometers from the meltwater plumes (Cowan and Powell, 1991). A number of recent studies focusing on the effects of Greenland's marine-terminating glaciers on primary production have found that, by upwelling nutrient-rich deep waters in the surface, these glaciers increase primary production in fjords (Cape et al., 2019; Hopwood et al., 2018; Juul-Pedersen et al., 2015; Meire et al., 2017, 2016). However, none of these studies have demonstrated the impact of tidewater-terminating glaciers on primary production within 10 km of the calving front, where suspended sediment concentrations are highest.

Warm waters intruding into the Arctic Ocean basin have also contributed to large decreases in sea ice extent and thickness in the 21st century (Carmack and Melling, 2011; Comiso et al., 2008; Kwok, 2018; Laxon et al., 2013; Onarheim et al., 2014; Serreze and Stroeve, 2015; Stroeve et al., 2012). Reduced sea ice coverage has significantly lengthened the growing season for phytoplankton by reducing early spring light limitation, contributing to a 30% increase in primary production in the Arctic Ocean between 1998 and 2012 (Arrigo et al., 2008; Arrigo and Dijken, 2015). Moreover, the thinning of sea ice and proliferation of melt ponds significantly increases the under ice light field (Perovich, 2018) and appears to have allowed for dramatic under-ice blooms to proliferate in certain parts of the Arctic. In the Chukchi Sea, Arrigo et al. (2014, 2012) observed early, extensive blooms in nutrient-rich continental shelf waters that had not been accounted for in previous estimates of Arctic primary production.

This study evaluates the impacts of warm Atlantic water influx in a fjord – and the sea ice loss and increased melting of a tidewater glacier that coincided with this influx – on the bio-optical and hydrographic properties in Kongsfjorden, Svalbard. Kongsfjorden, a well-studied fjord located in western Spitsbergen, has experienced increased Atlantic water influx since 2006 (Cottier et al., 2007) and hosts both boreal and Arctic flora and fauna due to glacial meltwater input at the head of the fjord (Hop et al., 2002). Changes in water mass formation and optics are assessed through two primary questions: 1) How has the intrusion of warm Atlantic water affected Kongsfjorden oceanography and water masses and 2) How are seasonal increases in glacial melting affecting near-ice face distribution of phytoplankton and hence, primary production? Field observations and remote sensing data inform a proposed conceptual model of the impacts of warm water influx on fjord primary production.

2. Methods

2.1. Study region

2.1.1. Physical context

Kongsfjorden, located at 79°N in the Norwegian territory of Svalbard (Fig. 1), is a 20 km-long fjord that runs from southeast to northwest on the western coast of Spitsbergen (Svendsen et al., 2002). The tide varies by less than 0.5 m in Kongsfjorden (Svendsen et al., 2002) and tidal height variation was minimal over this study. This fjord is considered representative of most other open fjords in the Arctic because of its lack of a bathymetric sill (although a narrow channel in the inner fjord prevents deep exchange with the outer fjord) and the strong Atlantic and glacial influences on its water masses (Hop et al., 2002).

Kongsbreen, Kronebreen, and Kongsvegen are tidewater glaciers that terminate in the southeast of Kongsfjorden (Fig. 1 B; Svendsen et al., 2002), producing ~1.4 km^3 of cold, fresh meltwater each year, primarily during the summer melt season (Svendsen et al., 2002). The fjord also has several terrestrially bound valley and cirque glaciers to the south, referred to as the Lovénbreane glacial complex, which have a mean annual velocity of −2 to −7 m yr^{-1} and provide a small input of meltwater and sediment to the fjord (Svendsen et al., 2002). Surface runoff contributes negligibly to fjord meltwater supply.

Kronebreen, which has a grounding line around 60 m depth (Sund et al., 2011), is the most rapidly retreating glacier in Kongsfjorden; it has a mean annual retreat velocity in the center of the front of −2 m d^{-1} and summer peak speeds of up to −4.5 m d^{-1} associated with increases in air temperature and rainfall (Lefauconnier et al., 1994; Luckman et al., 2015). In 2011, Kronebreen retreated 850 m and lost an area of 2.8 km^2, while nearby Kongsbreen retreated 1800 m between 2007 and 2013 and lost 2.5 km^2 (Schellenberger et al., 2015), a trend that will likely continue due to forecasted warming (Schellenberger et al., 2015; Trusel et al., 2010; Vallot et al., 2017). This rapid retreat coincided with the warming of the subsurface water in the fjord and the increase in sediment-rich meltwater draining from basal channels, which buoyantly upwells at the glacier-ocean interface and brings suspended sediment to the surface in seasonal sediment plumes (Luckman et al., 2015; Trusel et al., 2010). In the summer of 2014, a highly active persistent sediment plume was observed along the northern extent of Kronebreen in the same area as had been observed between 2009 and 2011 (Fig. 1 C; Rajagopalan, 2012). Additionally, there was intermittent sediment plume activity in front of the southern face of the Kongsbreen glacier, the southern portion of which has largely retreated onto bedrock since 2009 (Rajagopalan, 2012).

2.1.2. Oceanographic context

Two water masses originating outside of Kongsfjorden influence the hydrography of the fjord. The first of these, warm, saline Atlantic Water (AW; $T > 3$ °C, $S > 34.9$ psu), is transported northward along the shelf slope by the West Spitsbergen Current (WSC). The second is the colder, fresher Arctic Water (ArW; $T = 0.5$–2 °C, $S = 34.7$–34.9 psu; Hopkins, 1991), which flows northward on the shelf. Historically, AW transported onto the shelf mixed with ArW and formed the Transformed Atlantic Water (TAW; $T > 1$ °C, $S > 34.7$ psu) that flowed into the outer fjord of Kongsfjorden between 90 and 250 m (Svendsen et al., 2002). Interannual variability in the amount and characteristics of the TAW transported into Kongsfjorden (Cottier et al., 2005) occurred primarily as a function of prevailing local winds (Cottier et al., 2007; Nilsen et al., 2016). The characteristics of inflowing TAW have also been linked to sea ice extent in Nordic seas (Vinje, 2001) and thus the North Atlantic Oscillation (NAO), with low-drift ice years reducing on-shelf ArW and

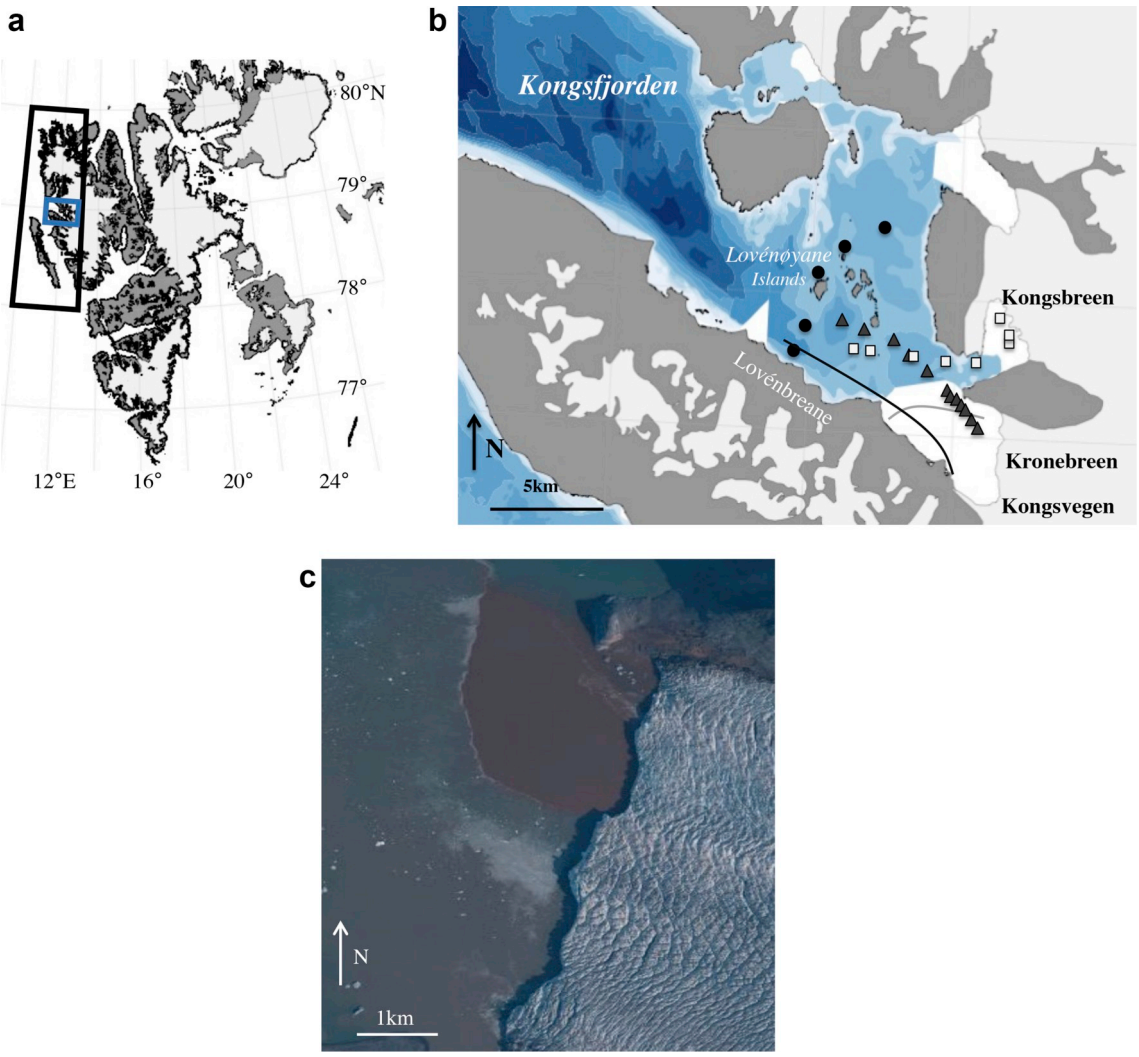

Fig. 1. Maps of (A) Svalbard, (B) Kongsfjorden, and (C) the Kronebreen glacial front. The black box in (A) indicates the region over which satellite data analysis was conducted, and the blue box demarcates the 2014 study site. In (B), the tidewater glaciers of this study are labeled in black text, while the terrestrial glaciers are labeled in white text. The three transects discussed in this paper emanate from three glaciers: Kongsbreen (white squares), Kronebreen (grey triangles), and Lovénbreane (black circles). Two other transects, A and D, are demarcated with a black and a grey line, respectively. A 2009 high-resolution image of Kronebreen glacier (C) shows that the persistent sediment plume impacts ocean color and iceberg distribution in the fjord. (For interpretation of the references to color in this figure legend, the reader is referred to the Web version of this article.)

thus creating warmer, more saline TAW. While TAW was transported into Kongsfjorden historically, conditions changed significantly in the winter of 2005/6 with an influx in AW into the inner fjord at a depth of 15 to 100 m (Cottier et al., 2007; Hegseth and Tverberg, 2013; Nilsen et al., 2016; Willis et al., 2008). Following this year, water observed in the fjord was indistinguishable from the AW core in the WSC (Aagaard et al., 1987). The increased ocean heat content associated with this anomalously warm water influx (Aliani et al., 2016) resulted in a permanent loss of winter sea ice starting in 2006 (Cottier et al., 2007; Onarheim et al., 2014) and changes in the timing, magnitude, distribution, and species composition of the spring phytoplankton bloom (Hegseth and Tverberg, 2013; Willis et al., 2008). Water transported into the fjord prior to 2006 will be referred to as TAW in this manuscript, while recent water in the fjord will be referred to as AW.

In addition to inflowing AW, there are two primary water masses present in the fjord (Hop et al., 2002 Fig. 2). The first, cold, fresh Surface Water (SW; $S < 34$ psu, T = variable, greater than 1 °C, 2–3 m thick), is produced through glacial melting (Fig. 2 A; Cottier et al., 2005; Svendsen et al., 2002). This SW layer has high turbidity associated with the sediment output of glaciers (Beszczyńska-Möller et al., 1997) and is highly mixed along the glacial front but creates a strong halocline in the outer fjord and prevents deep mixing (Svendsen et al., 2002). Historically, surface fjord water cooled significantly in the winter, forming sea ice, and the cold, salty water extruded during sea ice formation produced Winter Cooled Water (WCW; $T < -0.5$ °C, $S = 34.4–35$ psu), bottom water found in bathymetrically constrained pockets in the inner fjord (Fig. 2; Cottier et al., 2005; Svendsen et al., 2002).

2.2. In situ data collection

From August 4 to August 15, 2014, data were collected in Kongsfjorden, Spitsbergen. A SAIV A/S CTD/STD model SD204 (manufactured in Bergen, Norway), calibrated daily with a standard, with additional SAIV sensors measuring chlorophyll fluorescence and backscattering, was used to collect a survey of profiles (Fig. 1 B). Data were processed with the SD200W software packages. Over the 11 days of study, 53 casts were taken along 5 distinct transects separated by 0.25 to 2 km (Table 1).

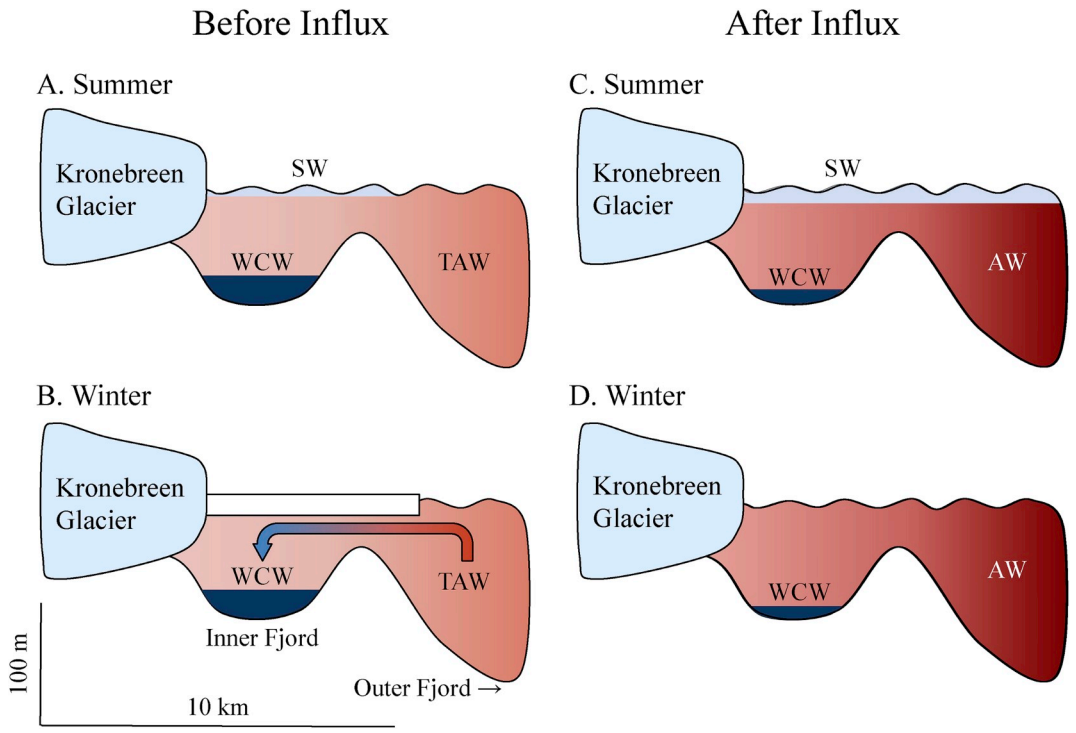

Fig. 2. Schematic of water masses in Kongsfjorden in the summer (top) and winter (bottom), before Atlantic Water (AW) influx (left; characterized by Hop et al., 2002) and after AW influx (right), with scale and relative fjord location demarcated in (B). Before AW influx (A), Transformed Atlantic Water (TAW) inflow in the summer coincided with Kronebreen glacier melting, which produced cold, fresh Surface Water (SW). In the winter (B), TAW cooled and extruded salt during sea ice production (cooling demonstrated by red to blue arrow), forming salty, cold Winter Cooled Water (WCW). After intrusion (C), the increased water temperature due to AW influx coincides with a summertime increase in the volume of SW due to increased glacial melting. This causes greater surface stratification in the inner fjord, preventing mixing until later in the season. Warmer waters prevent sea ice formation in the winter (D), changing the characteristics and concentration of WCW. (For interpretation of the references to color in this figure legend, the reader is referred to the Web version of this article.)

Table 1
Transect name, date, collection time, and details of cast numbers, names, and distances between the casts. * indicates high output, ^ indicates moderate output, while † indicates moderate plume activity after 5 inactive days.

Transect Name	Plume Dynamics	Date	# Casts	Range Chlorophyll a (mg m^{-3})	Range Turbidity (FTU)
Transect A	Southern portion of fjord; little plume activity	Aug. 6	7	0.01–0.78	0.5–47
Kongsbreen	Crosses intermittent plume † and persistent plume ^	Aug. 7	9	0.02–1.61	0.5–61
Kronebreen	Runs length of persistent plume *	Aug 9	13	0.04–1.75	0.5–122
Transect D	Runs length of persistent plume *	Aug. 11	6	0.02–0.35	2.0–90
Lovénbreane	Persistent plume * is over 7 km away	Aug. 14	5	0.03–7.61	0.2–12

2.3. Modeling the euphotic zone

Solar radiation decays exponentially with depth, and can be represented with an adaptation of Beer's law:

$$E(z) = E_0 e^{-k(z)*z} \quad (1)$$

where E_0 is surface irradiance, z is the depth of the euphotic zone (units, m) and k is the depth-dependent diffuse attenuation coefficient (units, m^{-1}; Kirk, 1994). The euphotic zone extends from the water surface to the depth at which the photosynthetically available radiation (PAR; the visible wavelength range, 400 nm–700 nm) is attenuated to 1% surface levels. By rearranging Eq. (1), the following approximates the euphotic depth, z_{eu}:

$$z_{eu} = \frac{\ln(0.01)}{-k(z)} \quad (2)$$

Solar radiation is attenuated in water due to both absorption and scattering. The absorption coefficient is determined by the optical properties of water itself and by its dissolved and particulate organic matter content, including phytoplankton. The scattering coefficient is determined by the molecular properties of seawater, and, more significantly, by the characteristics of the suspended organic and inorganic particles. In Kongsfjorden, suspended sediment and phytoplankton are the major contributors to particle scattering. Using a Monte Carlo simulation, Kirk (1994) quantified the attenuation coefficient as a function of the absorption (a) and scattering (b) coefficients in the following manner:

$$k = \left(a^2 + 0.256a * b\right)^{\frac{1}{2}} \quad (3)$$

Although photosynthetically available radiation, absorption, and backscattering were not measured *in situ* in this study, the euphotic depth can be modeled via well-established constituent-specific optical properties. This requires known profiles of optical constituents (in this case, chlorophyll fluorescence and turbidity) as well as published optical specific biogeochemical properties (Babin et al., 2003b).

In this study, the depth-dependent absorption coefficient (a; m^{-1}) is approximated by the sum of the contributions to absorption by seawater and by phytoplankton. This is because there is minimal dissolved or particulate organic material in Kongsfjorden waters (Hop et al., 2006; Stramski et al., 2007) as a result of sparse land vegetation (Svendsen et al., 2002; Pavlov et al., 2014) and because glacial sediments do not

contribute substantially to absorption (Stramski et al., 2007). Because this study investigates the attenuation of spectrally integrated irradiance in the visible wavelength range, the absorption profile is approximated by:

$$a(z) = a_{seawater} + F_{chl}(z)*0.018 \quad (4)$$

The spectrally integrated absorption by seawater ($a_{seawater}$) is given by the constant 0.2 m^{-1} (Smith and Baker, 1981) and F_{chl}, the depth-dependent value of the chlorophyll concentration, was measured with a calibrated profiling fluorometer (units, mg m^{-3}). The term 0.018 (units m^2 mg^{-1} chlorophyll) is the spectrally averaged value of the chlorophyll-specific absorption coefficient (Bricaud et al., 1995; Roesler and Barnard, 2013).

The scattering coefficient (b; m^{-1}) in Eq. (2) is approximated by the sum of the contributions to scattering by seawater and glacial sediments, as phytoplankton are relatively inefficient at scattering light compared to suspended sediments (Babin et al., 2003a). The scattering profile is approximated by:

$$b(z) = b_{seawater} + T_{sed}(z)* \frac{0.00408}{0.03} \quad (5)$$

The spectrally integrated scattering by seawater ($b_{seawater}$) is given by the constant 0.007 m^{-1} (Morel and Morgan, 1972). The second term represents the particle scattering coefficient, where $T_{sed}(z)$ is the depth-dependent turbidity obtained by a calibrated turbidity sensor (measured in Formazin Turbidity Units, or FTU). The constant 0.00408 is the formazin-specific backscattering coefficient (FTU), which converts calibrated turbidity to the backscattering coefficient (WETLabs turbidity/backscattering sensor manual), and 0.03 is the particle backscattering ratio, or the fraction of total particle scattering that is in the backwards direction. The backscattering ratio varies from about 0.5% for phytoplankton to 1% for detrital organic particles and 3% for inorganic sediments (Twardowski et al., 2001). Because glacial sediments dominated the particle field in these waters, a relatively high backscattering ratio of 3% was used for euphotic depth calculations in this study.

2.4. MODIS satellite data

Satellite analyses and visualizations used in this study were produced with the Giovanni Ocean Color Radiometry Online Visualization and Analysis data system, developed and maintained by the NASA Goddard Earth Sciences Data and Information Services Center (GES DISC; Acker and Leptoukh, 2007). A large spatial region was chosen because reduced analysis size produced a disjointed time series due to cloudiness and the short portion of the year with daylight. The 4-km MODIS-Aqua 8 day mean satellite sensor observations were used to analyze changes to SST (°C) and chlorophyll *a* concentrations (mg m^{-3}) between July 2002 and October 2018. SST observations were made using nighttime-only 11 μm channel observations in non-summer months but combined nighttime and daytime measurements in months with continuous light to ensure minimal day-night bias. The GSM inherent optical property inversion results in estimates of particulate backscattering at 440 nm (m^{-1}) and non-algal absorption at 440 nm (m^{-1}) (i.e., absorption by non-algal particulate and colored dissolved organic matter, often referred to as detrital absorption, a_{dg}) obtained at 9 km resolution, were used to analyze changes in particulate backscattering and absorption between 2003 and 2010. The monthly averaged timeseries were spatially averaged over the area from 78° to 80°N and 10° to 13°E (Fig. 1 A). Monthly and seasonal means were calculated and reported when trends over the time series were significant. Time series trend data were compared using linear regressions computed in R.

3. Results

3.1. Water masses

Three distinct water masses were observed in Kongsfjorden in August 2014: Surface Water (SW; T = 1–5 °C, S < 34.7 psu, 1–15 m); Atlantic Water (AW; T = 5.5–7 °C, S > 34.9 psu, 15–60 m); and Winter-Cooled Water (WCW; T < 1.5 °C, S > 34.9 psu, 30–60 m; Fig. 3). SW characteristics were within the range of variability observed historically and extended to ~10 m depth. Water masses observed in 2014 were significantly warmer than historical observations of TAW (the AW observed here represents a 4–5.5 °C and 0.15 psu increase over previous typical temperatures and salinities) and WCW (1–2 °C and ~0.6 psu increase over previous temperatures and salinities) in the fjord (Svendsen et al., 2002). Stratification was driven by salinity differences in SW and AW, while temperature was more significant in stratification between AW and WCW.

3.2. Euphotic depth

The depth of the 1% light level, or the euphotic depth, was modeled for all casts, and occurred between 4 and 21 m (Fig. 4). Variability in the absorption and backscattering of light through the water column affected the euphotic depth across Kongsfjorden (Fig. 5). Chlorophyll *a* concentrations varied from approximately 0 to 7.5 mg m^{-3}, with maxima primarily in the upper 10 m. Turbidity varied from 0 to 140 FTU, with maxima typically between 0 and 15 m. Chlorophyll *a* concentrations did not surpass 0.5 mg m^{-3} when turbidity was above 20 FTU. Across most transects, light attenuation was primarily influenced by turbidity.

3.3. Hydrographic transects

A day of high persistent plume flow was observed on August 9th, 2014 along the Kronebreen transect (Figs. 1 B and 4 A-C), as evidenced by a skin of cool surface water (1–2.5 °C) atop significantly warmer water (5.5–6 °C) at intermediate depths (~25 m–80 m). With turbidity values exceeding 120 FTU through much of the sediment plume, this transect had high suspended sediment in the water column more than 5 km from the glacier face, with clear evidence of sinking particles away from the glacial source. The euphotic zone shoaled to 7 m in the persistent plume but reached a depth of 21 m at the far extent of the

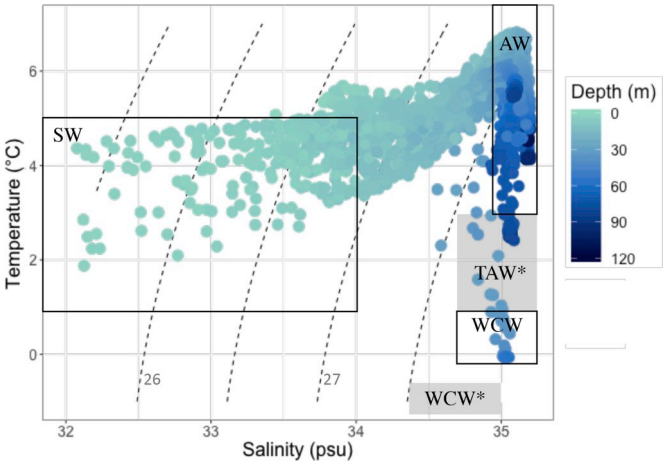

Fig. 3. T-S diagram for all casts, colored by depth, for salinity values from 32 ppt to 35.5 ppt and temperatures −1 °C–7 °C. Black boxes indicate the T-S characteristics of the water masses measured in 2014, as described in Fig. 2, while grey boxes and (*) indicate historical ranges (Svendsen et al., 2002): Surface Water (SW), Transformed Atlantic Water (TAW), and Winter Cooled Water (WCW).

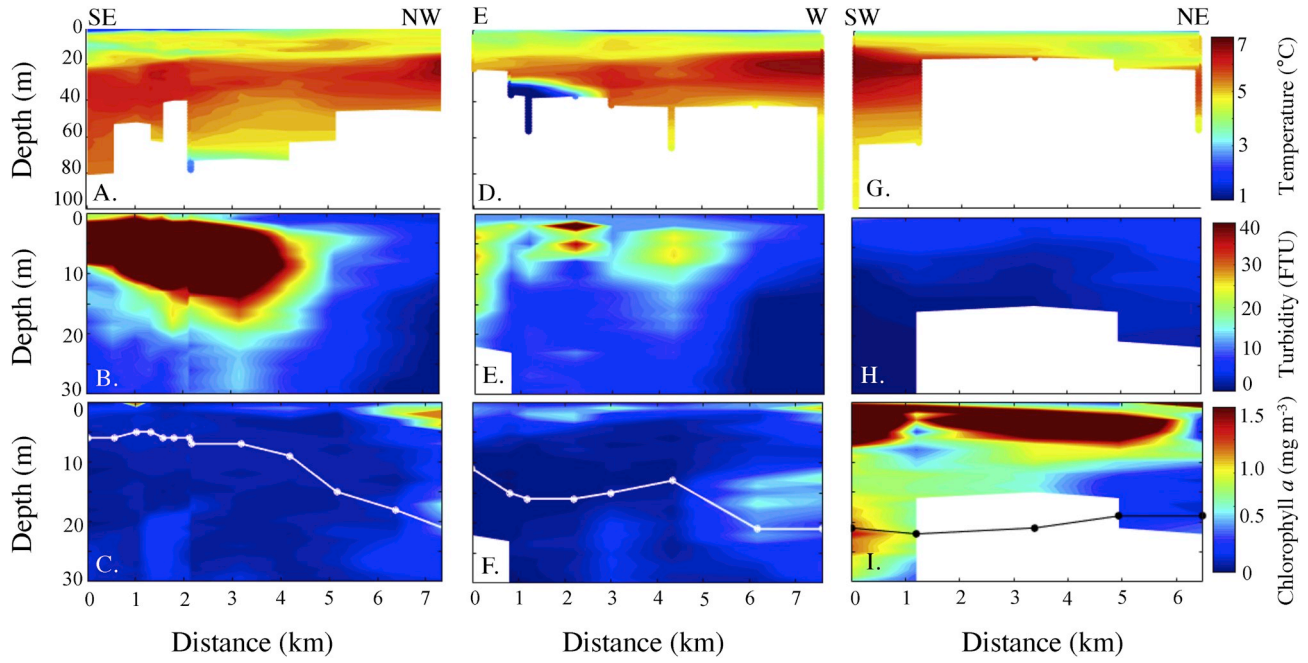

Fig. 4. Interpolated contour plots of transects of water conditions with distance from Kronebreen (A–C), Kongsbreen (D–F) and Lovénbreane (G–I) glaciers (on left of each plot), with color representing temperature over 100 m (A, D, G), turbidity over 30 m (B, E, F), and chlorophyll *a* over 30 m (C, F, I). The white lines (C, F) and black line (I) show the modeled euphotic zone depth. The grey arrow above (D) indicates the intermittent plume location, while the black arrows (A, D) indicates the consistent plume location. Contour plots A, B, and C show conditions associated with distance from a consistent sediment plume on a high output day; D, E, and F show characteristics associated with an intermittent sediment plumes on a moderate-output day after 5 inactive days and a consistent plume on a moderate-output day; and G, H, and I show conditions associated with proximity to sediment plumes produced by land-terminating glaciers.

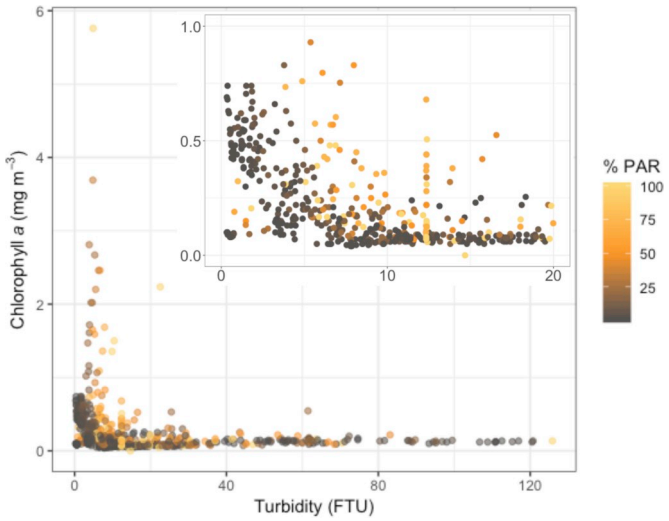

Fig. 5. Relationship between paired chlorophyll *a* (mg m^{-3}) and turbidity (FTU) observations from all casts, color-coded by % PAR. Inset is constrained to chlorophyll *a* concentrations between 0 and 1 mg m^{-3} and turbidity values between 0 and 20 FTU. Chlorophyll *a* is negatively correlated with turbidity, and only has peak values when turbidity is less than 20 FTU. (For interpretation of the references to color in this figure legend, the reader is referred to the Web version of this article.)

transect, coinciding with chlorophyll *a* concentrations exceeding 1.8 mg m^{-3} from 0 to 10 m and a smaller subsurface maximum of 0.6 mg m^{-3} at about 20 m.

The Kongsbreen transect, taken on August 6th, 2014 on a day of moderate intermittent plume flow preceded by several days of no output, crossed both the intermittent plume in front of Kongsbreen and the persistent sediment plume in front of Kronebreen on a day of moderate output (Figs. 1 B and 4 D-F). Temperatures were warm at the surface (3–4 °C), warmer at an intermediate depth of 25–50 m (5–6 °C), and coldest at depth in the inner fjord (−0.2 °C; Fig. 4 D). Despite turbidity of ~60 FTU near Kongsbreen, chlorophyll *a* values of 0.65 mg m^{-3} were found at a depth of 3 m between two distinct turbidity layers but well within the euphotic zone at the intermittent plume; however, consistent sediment plume output of lower-turbidity water (~25 FTU) from the Kronebreen glacier was associated with lower chlorophyll *a* (0.2 mg m^{-3}). The highest and deepest distributions of chlorophyll *a* were found farther from the glacier (>6 km), where reduced turbidity (12 FTU, rather than 40 + FTU; Fig. 4) deepened the euphotic zone.

The Lovénbreane transect (Figs. 1 B and 4 G-I) taken on August 14th ranged from 0.5 to 7 km from the terrestrially-terminating Lovénbreane glaciers, which typically don't have substantial sediment plumes. This transect had a thin skin of SW (3–4.5 °C), AW at 25 m (5.5–7 °C) and the lowest turbidity values in the top 20 m (10–12 FTU) of any transect (Fig. 4). Because of the low turbidity, the euphotic depth remained persistently deep throughout the transect, and chlorophyll *a* concentrations were high throughout, with values as high as 7.5 mg m^{-3}.

3.4. Satellite data

Remote sensing data are over a much larger region than *in situ* observations and thus demonstrate regional trends rather than reflecting intra-fjord dynamics. A comparison of annual SST timeseries from 2002 to 2018 reveals that winter temperatures are typically between 1 and 3 °C, while summer temperatures peak between 4 and 7 °C (Fig. 6 A). Satellite-derived SST anomalies indicate that there has been a 0.85 °C temperature increase per decade between 2002 and 2018 ($p < 0.001$, $R^2 = 0.11$; Fig. 7 A). Changes in mean summer and fall temperatures drove this warming; mean summer temperatures (Jul/Aug/Sept) increased from 4.4 °C between 2002 and 2004 to 5.7 °C between 2016 and 2018, while mean fall temperatures (Oct/Nov/Dec) increased from 1.5 °C to 3 °C over the same period. Satellite data indicate that SST in the summer of 2014, the year of field work, was the 3rd warmest on record

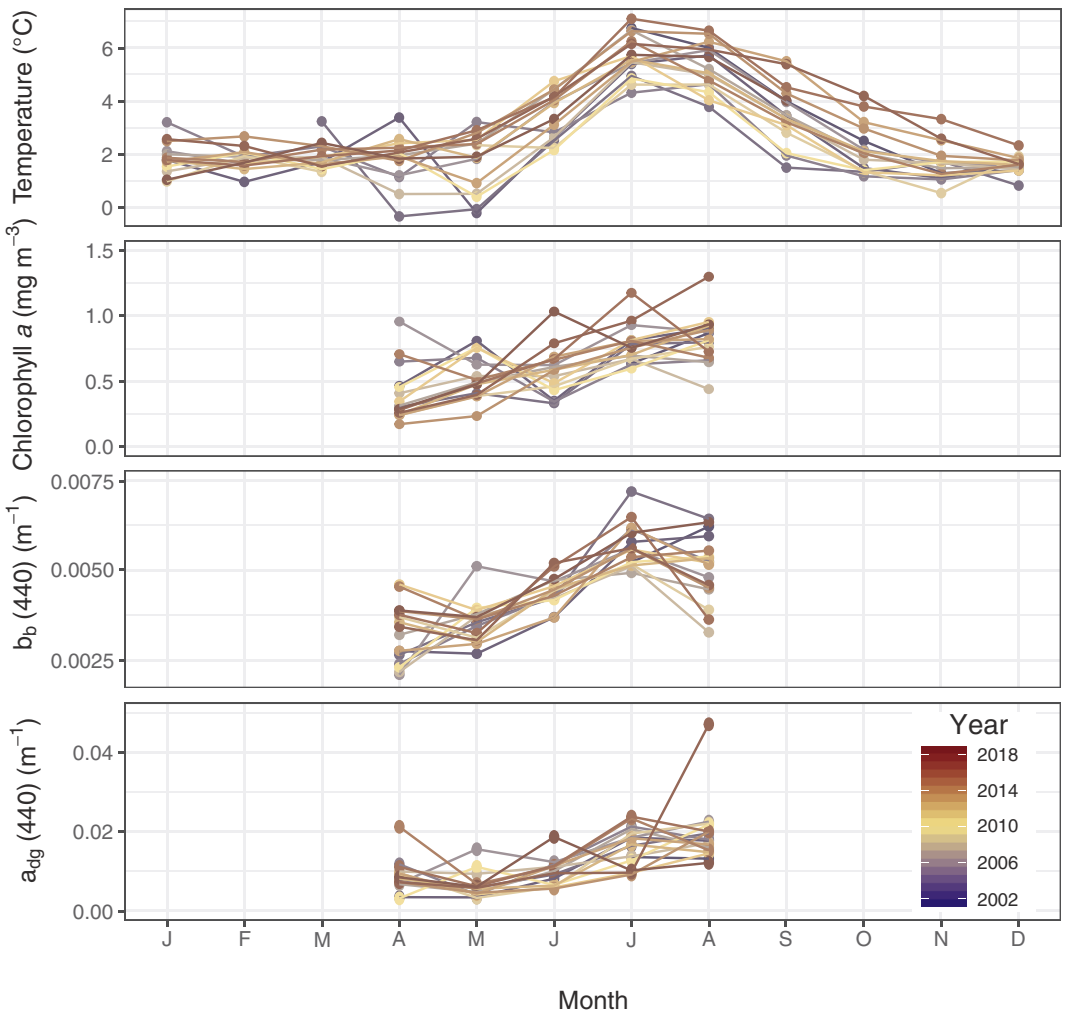

Fig. 6. Monthly-averaged time series of MODIS-Aqua 4 km 8-day products spatially averaged over the area from 78° to 80N and 10° to 13° E (black box in Fig. 1 A) for (A) sea surface temperature (°C), (B) chlorophyll *a* concentration (mg m^{-3}), (C) particulate backscattering at 440 nm (m^{-1}), and (D) absorption by detritus and colored dissolved organic matter (CDOM) at 440 nm (m^{-1}) for 2002–2018.

(Fig. 6 A).

Chlorophyll *a* concentrations in surface waters varied from about 0.2 to 1.3 mg m^{-3} between 2002 and 2018, with climatological values gradually increasing between April and August (Fig. 6 B). The highest spring chlorophyll *a* concentrations was observed in April of 2006 (1 mg m^{-3}) as the result of an early-season maximal bloom, while the highest overall chlorophyll *a* concentration occurred in August of 2017 (1.3 mg m^{-3}; Fig. 7 B). Chlorophyll *a* concentrations peaked in August prior to 2006, in April in 2006, and in July and August following 2006. June chlorophyll *a* concentrations increased over the time series ($R^2 = 0.66$, $p = 0.0001$), but there were no significant trends in other months.

Particulate backscattering ranged from 0.002 to 0.007 m^{-1}, with values increasing over the summer months and peaking in July and August, at the height of the glacial melt season (Fig. 6 C). There was no statistically significant change in the intensity of the backscattering coefficient over the timeseries (Fig. 7 C). However, there was a slight increase in April backscattering over the course of the time series ($R^2 = 0.40$, $p = 0.008$).

Absorption by detrital matter ranged from 0 to 0.03 m^{-1}, with values increasing slightly over summer months and peaking in August, which also was the month of highest variance (Fig. 6 D). These low values for detrital absorption indicate that it is not a significant absorber of light and thus not an important consideration in quantifying euphotic depth.

4. Discussion

4.1. Water temperature and water mass structure in Kongsfjorden

The results of this study confirm that there are three primary water masses found in Kongsfjorden: cool, fresh SW formed by glacial meltwater; salty, warm AW; and cold, salty WCW bathymetrically constrained to the inner fjord. The SW layer appears to be slightly warmer and fresher than previous estimates, but SW has always had variable characteristics. It does seem substantially thicker than between 1996 and 1999 (Svendsen et al., 2002), exceeding 10 m in thickness even 5 km from the nearest tidewater glacier. There have been more substantial changes in characteristics of the inflowing AW and the bottom water, WCW. While from 1996 to 1999, Transformed Atlantic Water temperatures were between 1.5 and 2 °C during the summer field season (Svendsen et al., 2002), more recent studies in Kongsfjorden found significant warming trends. The 5–6.5 °C inflowing water observed in 2014 indicates that AW, rather than TAW, has flowed into Kongsfjorden since 2006. As for the WCW, there has been a 2 °C increase in temperature and a 0.6 psu increase in salinity since 1999, and a reduction in volume since 2011 (Rajagopalan, 2012). The characteristic and volume changes are also likely associated with the change in inflowing water, from cooler, fresher TAW to warmer, saltier AW. While WCW has historically formed due to winter cooling and sea ice formation near the tidewater glaciers, AW inflow has prevented sea ice formation since

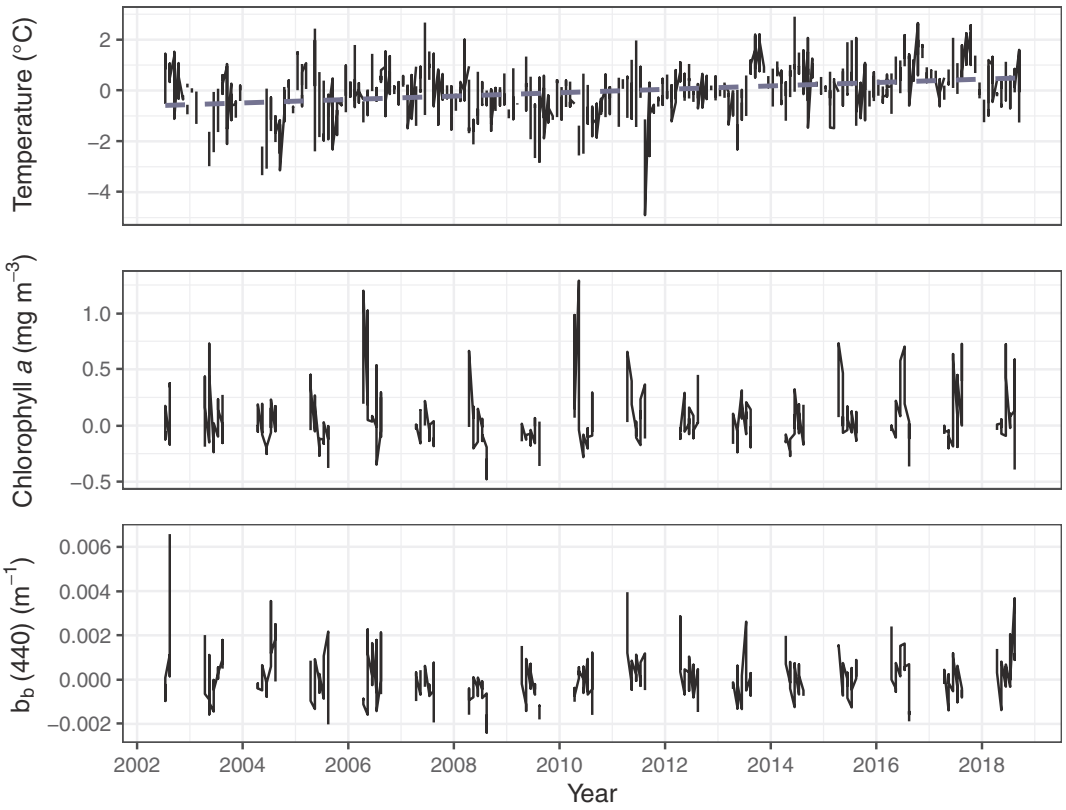

Fig. 7. MODIS-Aqua 4 km 8-day (black points) satellite anomalies spatially averaged over the area from 78° to 80°N and 10° to 13° E (black box in Fig. 1 A) for (A) sea surface temperature (°C), (B) chlorophyll *a* concentration (mg m^{-3}), (C) particulate backscattering at 440 nm (m^{-1}), and (D) absorption by detritus and colored dissolved organic matter (CDOM) at 440 nm (m^{-1}) for 2002–2018. Blue dashed line indicate linear regression when significant. (For interpretation of the references to color in this figure legend, the reader is referred to the Web version of this article.)

2006 (Hegseth and Tverberg, 2013; Willis et al., 2008), and WCW has instead likely formed through convective cooling of AW, explaining its warmer, more saline characteristics.

In addition to a warming of the inflowing water mass in the fjord, satellite-derived SST indicates that regional surface water temperatures warmed around 1.2 °C between 2002 and 2018 primarily due to warming in summer and fall, with fall temperatures from 2016 to 2018 averaging 1.5 °C warmer than between 2002 and 2005 (Fig. 7A). Satellite SST cannot elucidate how temperatures are changing at depth or within a given water mass. However, these data indicate that conditions in the summers of 2016 and 2014 were the warmest between 2002 and 2018, which may indicate a reduction in glacial melt water in the region or an increase in AW in the surface waters of the shelf.

4.2. The euphotic zone

The hydrographic transects collected as a part of this study indicate that proximity to a rapidly retreating glacier has substantial impacts on the distribution of phytoplankton and, by inference, primary production. Particulate backscattering, which is correlated to glacial output/retreat, played a larger role than absorption by chlorophyll *a* in determining the depth of the euphotic zone. Calculations of the euphotic zone were made with the assumption that there was minimal contribution of detrital organic material to the fjord (Hop et al., 2006; Pavlov et al., 2014; Stramski et al., 2007; Svendsen et al., 2002), which was supported by regional satellite analysis (Fig. 6D), and previous work indicating that glacial sediments do not substantially absorb PAR (Babin et al., 2003b; Stramski et al., 2007). If this assumption is incorrect, the euphotic zone may be shallower than the current model indicates. Regardless, turbidity plumes originating from tidewater glaciers were observed to limit the depth of the euphotic zone while proximity to river output from terrestrially-terminating glaciers did not affect euphotic depth.

4.3. Hydrographic transects

4.3.1. Persistent sediment plume

The turbidity in the persistent sediment plume was extremely elevated close to Kronebreen glacier (with values as high as 140 FTU ~500 m from the glacier terminus) but diminished with distance as sediments flocculated and sunk out of the water column (20 FTU at 5 km from the glacier terminus). A suspended sediment load of this magnitude causes a shoaling of the euphotic zone such that 1% PAR values occur at a depth of 5–10 m in the center of the plumes. Because light attenuation was high within the persistent sediment plume, chlorophyll *a* values were below 0.3 mg m^{-3} and water column integrated primary production was likely limited. However, decreased suspended sediment around 5 km from the glacier caused the euphotic zone to increase in depth, and increased chlorophyll *a* throughout the euphotic zone suggested higher integrated primary production.

4.3.2. Intermittent sediment plume

Unlike the high-turbidity conditions in persistent sediment plumes and the low-turbidity conditions found proximal to land-terminating glaciers, the effects of intermittent plumes on phytoplankton are challenging to characterize due to their unstable nature and the time scales of plume variability relative to the time scales of phytoplankton production. The intermittent plume near Kongsbreen at times resembled the persistent plume to the south, where high turbidity concentrations reduced the euphotic depth to < 10 m, limiting phytoplankton production up to ~ 5 km from the glacier. However, moderate chlorophyll *a* concentrations persisted near these intermittent plumes when there was

low plume activity. The Kongsbreen transect occurred on a day of moderate intermittent plume input following 5 inactive days; two distinct layers of turbid meltwater were observed at 2 and 7 m, above and below a moderate phytoplankton bloom (from 2–4 m). Although the phytoplankton were located well above the euphotic zone, this particular bloom was still susceptible to mixing below the 1% PAR depth.

Phytoplankton near intermittent plumes are subject to variable, inhospitable conditions. While cessation of plume activity may allow phytoplankton to bloom briefly, meltwater input might lead to a sudden shoaling of the euphotic zone, causing stable populations to subduct under the euphotic depth or become confined to the surface waters. Fresh, low-density water upwelling from the base of the glacier may increase the supply of nutrients in the surface waters as has been observed in Greenland's tidewater glaciers (Hopwood et al., 2018; Juul-Pedersen et al., 2015; Meire et al., 2017, 2016). However, upwelling simultaneously enhances mixing proximal to the ice front, making populations located above the euphotic depth susceptible to deep mixing. In addition, phytoplankton in Kongsfjorden surface waters and throughout the Arctic are exposed to high levels of UV radiation. In areas of high UV light radiation, such as the polar regions, limited mixing of phytoplankton away from the surface can cause photodamage and death (Neale et al., 1998). UV-B light has been observed to penetrate up to 13 m in Kongsfjorden (Svendsen et al., 2002) and could have a strong negative impact on primary producers (Helbling et al., 1996; Hop et al., 2002). In near-glacier areas where the euphotic zone is restricted to the surface 10 m and where mixing is limited by the strong stratification of surface waters, phytoplankton populations are unlikely to persist.

4.3.3. No sediment plume

Across all transects, high chlorophyll *a* values were found exclusively in low turbidity, low sediment conditions. In the Lovénbreane transect (7 km from the nearest tidewater glacier, 2 km from nearest terrestrial glaciers), turbidity values were below 12 FTU, an order of magnitude lower than within the sediment plume. Due to the stable and deep euphotic depth, which ranged from 19 to 21 m, chlorophyll *a* concentrations of up to 7.5 mg m^{-3} were measured, showing that the region is capable of high primary production when turbidity levels are low. Although land-terminating glaciers input small amounts of fresh water and sediment to the fjord through rivers, phytoplankton appear uninhibited by the meltwater input of terrestrial glaciers and appear, in fact, flourish in the salinity-induced stratification.

4.4. Satellite evidence of changes to primary productivity and glacial melting

Regional satellite measurements of chlorophyll *a* indicate that in 2006, the year of warm water intrusion and sea ice loss in the fjord, the larger region experienced anomalously high chlorophyll *a* concentrations driven by an April bloom, followed by reduced chlorophyll concentrations from 2007 to 2009. A mooring in Kongsfjorden indicates that these trends were also observed in the fjord (Hegseth and Tverberg, 2013). Increased spring chlorophyll concentrations in the fjord in 2006 have been attributed to increased light availability due to sea ice loss, while a reduction in chlorophyll *a* in 2007 and 2008 was attributed to a lack of nutrients in surface waters.

There were no significant changes in the regional particulate backscattering coefficient between 2002 and 2018. Backscattering in Kongsfjorden was dominated by glacially-derived sediment between 5 and 15 m, but regional backscattering might not be dominated by glacially-derived particles and would not reflect changes occurring below the surface. Particulate backscattering is lowest in the spring and highest in the summer, tracking the seasonal cycle of glacial melting in the fjord.

4.5. Conceptual model for warm-water intrusion

We have developed a conceptual model to describe the impacts of warm-water intrusions in Arctic fjords on water characteristics and primary production within 10 km of retreating tidewater glaciers (Fig. 8). When intruding waters in a fjord warm substantially, a sudden loss of sea ice can occur, as was observed in 2006 in Kongsfjorden (Nilsen et al., 2016; Onarheim et al., 2014). Because sea ice production is a critical part of the bottom water formation process, this will likely impact the water mass dynamics of most fjords, changing the quantity and characteristics of bottom waters as in Kongsfjorden. When sea ice coverage decreases, phytoplankton face less light limitation by overlying sea ice in the spring, allowing blooms to occur earlier, although low nutrients in the inflowing AW may reduce the bloom magnitude (Hegseth and Tverberg, 2013). Satellite data and field observations from the Kongsfjorden region (Cottier et al., 2007; Willis et al., 2008) indicates that substantial increases in SST and increased chlorophyll *a* concentrations both occurred in 2006.

In fjords with tidewater-terminating glaciers such as Sermek Kujalleq, warm water intrusion was followed by sea ice loss and subsequent increased glacial melt and retreat (Joughin et al., 2014). Increased inputs of glacial meltwater in fjords with shallow tidewater glaciers can increase salinity-driven stratification (Mortenson et al., 2018), affecting water mass formation by delaying surface cooling and convective mixing until later in the fall or winter. As shown in both the persistent and intermittent sediment plumes of the Kronebreen and Kongsbreen transects, phytoplankton are likely unable to persist within 5 km of a marine-terminating glacier when glacial melt production is high. Although some small-scale primary production may occur near intermittent plumes, increased glacial melting generally corresponds to a reduction in phytoplankton blooms within 5 km of glaciers.

When warm waters intrude into a fjord and contribute to increased glacial retreat, tidewater glaciers may ablate into deeper basins, exposing a larger portion of their ice face to the water and leading to further melting (Holland et al., 2008). Although glaciers that act as outlets for ice caps (such as those in Greenland and Antarctica) have the potential to retreat for decades to centuries, many glaciers will eventually retreat onto land, becoming terrestrially terminating. When this happens, overall glacial melt rates and the sediment and fresh water input into the fjord are likely reduced. In relatively shallowly-grounded tidewater glaciers, where meltwater plumes reach the surface waters, the loss of glacial meltwater in the fjord may reduce stratification during the summer, increasing winter mixing and potentially allowing sea ice and bottom water formation again. During this stage of warm water intrusion, approximated in this study through the Lovénbreane transect, primary production should increase, with phytoplankton blooms occurring earlier in the season than before sea ice coverage was lost.

Like Kongsfjorden, many Arctic fjords exposed to Atlantic water currently have a gradient of species distributions, with Arctic-type species close to the glaciers and Atlantic-type species near the mouth of the fjord. Because post-glacial retreat blooms will occur in warmer waters, Atlantic phytoplankton populations will likely outcompete the Arctic species that have previously dominated these fjords (Hegseth and Tverberg, 2013; Willis et al., 2008). Sea ice loss and earlier blooms could potentially cause timing mismatches with zooplankton (Willis et al., 2008), which may have ramifications for upper-trophic level feeders. Further research into the effects of warm water intrusion on these upper-trophic level species is a critical next step.

Intrusion of warm waters has been correlated with glacial retreat in the polar regions. From 2000 to 2010, Greenland's glaciers retreated over 267 km, with only 5.5% of glaciers on the continent advancing (Murray et al., 2015). Retreat of large tidewater glaciers in Greenland has largely been hypothesized to occur because of ocean and atmospheric forcing (Cowton et al., 2018), particularly in East Greenland. Additionally, glaciers in the Antarctic increasingly appear to be subject to the effects of warming waters. Ice shelf collapse events in the West

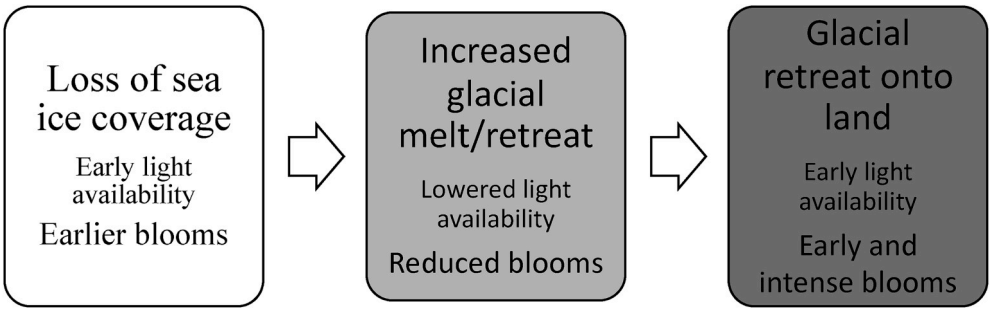

Fig. 8. Conceptual model for the impacts of warm-water intrusion on water characteristics, the optical light field, and primary production within 10 km of tidewater glaciers proposed as a part of this study.

Antarctic Peninsula are increasing and have been attributed to increased oceanic heat flux, basal melting and destabilization (Cook et al., 2016; Sallee, 2018). Understanding how warm water intrusion is impacting fjord ecosystems is imperative to assessing how these regions are changing. Future work should more accurately determine what factors allow for intrusion, measure its impacts on phytoplankton physiology and community composition, and regionally evaluate how sea ice, bottom water formation, water column sediment load, and primary production change as a result of warm water intrusion.

5. Conclusions

In Kongsfjorden, the intrusion of Atlantic Water, rather than a mixture of Atlantic and Arctic waters, warmed subsurface waters by 4–5.5 °C in a mere 15 years. This co-occurred with a loss of sea ice, rapid glacial retreat, changed water column structure, and changes in chlorophyll *a* in the region. Measurements from the summer of 2014 and a 16-year satellite dataset allowed for a temporal understanding of changes in this region inform a conceptual model for the impacts of warm water intrusion on near-glacial primary production. First, sea ice loss following warm water intrusion allows earlier phytoplankton blooms to occur and can change the water mass structure of the fjord. Second, glacial melting increased, reducing light availability thus primary production within 5 km of the glacier. Finally, as tidewater glaciers retreat onto land, light availability will increase, allowing early and intense phytoplankton blooms.

Declaration of competing interest

The authors declare that they have no known competing financial interests or personal relationships that could have appeared to influence the work reported in this paper.

Acknowledgements

This research was conducted with support from NSF's Research Experience for Undergraduates (REU) program (#0649006), Bowdoin College's Grua/O'Connell fellowship and the NASA Ocean Biology and Biogeochemistry Program. Thanks also to Julie Brigham-Grette, Ross Powell, and those at the Kings Bay Marine Laboratory for their assistance with the fieldwork. Satellite remote sensing data provided by NASA Goddard Space Flight Center, Ocean Ecology Laboratory, Ocean Biology Processing Group. Moderate-resolution Imaging Spectroradiometer (MODIS) Aqua 2018 Reprocessing. NASA OB.DAAC, Greenbelt, MD, USA for Chlorophyll Data (https://doi.org/10.5067/AQUA/MODIS/L3B/CHL/2018), Garver-Siegel-Maritorena (GSM) Model Data (https://doi.org/10.5067/AQUA/MODIS/L3M/GSM/2018) and Sea Surface Temperature Data (https://doi.org/10.5067/AQUA/MODIS/L3M/SST/2014), accessed 11/07/2018. We are very grateful to the two anonymous reviewers. Their constructive criticism and encouragement improved this manuscript significantly.

References

Aagaard, K., Foldvik, A., Hillman, S.R., 1987. the West spitsbergen current: disposition and water mass transformation. J. Geophys. Res. Ocean 92, 3778–3784. https://doi.org/10.1029/JC092iC04p03778.

Acker, J.G., Leptoukh, G., 2007. Online analysis enhances use of NASA Earth science data. Eos (Washington. DC) 88, 14–17. https://doi.org/10.1029/2007EO020003.

Aliani, S., Sciascia, R., Conese, I., D'Angelo, A., Del Bianco, F., Giglio, F., Langone, L., Miserocchi, S., 2016. Characterization of seawater properties and ocean heat content in Kongsfjorden, Svalbard Archipelago. Rendiconti Lincei. Sci. Fis. Nat. 27, 155–162. https://doi.org/10.1007/s12210-016-0544-4.

Arrigo, K., Perovich, D.K., Pickart, R.S., Brown, Z.W., van Dijken, G.L., Lowry, K.E., Mills, M.M., Palmer, M.A., Balch, W.M., Bahr, F., Bates, N.R., Benitez-Nelson, C., Bowler, B., Brownlee, E., Ehn, J.K., Frey, K.E., Garley, R., Laney, S.R., Lubelczyk, L., Mathis, J., Matsuoka, A., Mitchell, B.G., Moore, G.W.K., Ortega-Retuerta, E., Pal, S., Polashenski, C.M., Reynolds, R.A., Schieber, B., Sosik, H.M., Stephens, M., Swift, J. H., 2012. Massive phytoplankton blooms under arctic sea ice. Science 336, 1408 (80-.).

Arrigo, K., Perovich, D.K., Pickart, R.S., Brown, Z.W., van Dijken, G.L., Lowry, K.E., Mills, M.M., Palmer, M.A., Balch, W.M., Bates, N.R., Benitez-Nelson, C.R., Brownlee, E., Frey, K.E., Laney, S.R., Mathis, J., Matsuoka, A., Greg Mitchell, B., Moore, G.W.K., Reynolds, R.A., Sosik, H.M., Swift, J.H., 2014. Phytoplankton blooms beneath the sea ice in the Chukchi sea. Deep. Res. Part II Top. Stud. Oceanogr. 105, 1–16. https://doi.org/10.1016/j.dsr2.2014.03.018.

Arrigo, K., van Dijken, G., Pabi, S., 2008. Impact of a shrinking Arctic ice cover on marine primary production. Geophys. Res. Lett. 35, 1–6. https://doi.org/10.1029/2008GL035028.

Arrigo, K., van Dijken, G.L., 2015. Continued increases in Arctic Ocean primary production. Prog. Oceanogr. 136, 60–70. https://doi.org/10.1016/j.pocean.2015.05.002.

Arrigo, K., van Dijken, G.L., Bushinsky, S., 2008. Primary production in the southern ocean, 1997-2006. J. Geophys. Res. Ocean 113, 1997–2006. https://doi.org/10.1029/2007JC004551.

Babin, M., Morel, A., Fournier-Sicre, V., Fell, F., Stramski, D., 2003. Light scattering properties of marine particles in coastal and open ocean waters as related to the particle mass concentration. Limnol. Oceanogr. 48, 843–859.

Babin, M., Stramski, D., Ferrari, G., Claustre, H., Bricaud, A., Obolensky, G., Hoepffner, N., 2003. Variations in the light absorption coefficients of phytoplankton, nonalgal particles, and dissolved organic matter in coastal waters around Europe. J. Geophys. Res. 108 https://doi.org/10.1029/2001JC000882.

Bekryaev, R.V., Polyakov, I.V., Alexeev, V.A., 2010. Role of polar amplification in long-term surface air temperature variations and modern arctic warming. J. Clim. 23, 3888–3906. https://doi.org/10.1175/2010JCLI3297.1.

Beszczyńska-Möller, A., Węsławski, J.M., Walczowski, W., Zajączkowski, M., 1997. Estimation of glacial meltwater discharge into Svalbard coastal waters. Oceanologia 39, 289–299. https://doi.org/10.1111/j.1365-2664.2005.01126.x.

Bricaud, A., Babin, M., Morel, A., Claustre, H., 1995. Variability in the chlorophyll-specific absorption coefficients of natural phytoplankton: analysis and parameterization. J. Geophys. Res. 100, 13321–13332. https://doi.org/10.1029/95JC00463.

Cape, M.R., Straneo, F., Beaird, N., Bundy, R.M., Charette, M.A., 2019. Nutrient release to oceans from buoyancy-driven upwelling at Greenland tidewater glaciers. Nat. Geosci. 12, 34–39. https://doi.org/10.1038/s41561-018-0268-4.

Carmack, E., Melling, H., 2011. Warmth from the deep. Nat. Geosci. 4, 7–8. https://doi.org/10.1038/ngeo1044.

Comiso, J.C., Parkinson, C.L., Gersten, R., Stock, L., 2008. Accelerated decline in the Arctic sea ice cover. Geophys. Res. Lett. 35, 1–6. https://doi.org/10.1029/2007GL031972.

Cook, A.J., Holland, P.R., Meredith, M.P., Murray, T., Luckman, A., Vaughan, D.G., 2016. Ocean forcing of glacier retreat in the western Antarctic Peninsula. Science 353, 283–286. https://doi.org/10.1126/science.aae0017 (80-.).

Cottier, F., Tverberg, V., Inall, M., Svendsen, H., Nilsen, F., Griffiths, C., 2005. Water mass modification in an Arctic fjord through cross-shelf exchange: the seasonal hydrography of Kongsfjorden. Svalbard. J. Geophys. Res. Ocean. 110, C12005. https://doi.org/10.1029/2004JC002757.

Cottier, F.R., Nilsen, F., Inall, M.E., Gerland, S., Tverberg, V., Svendsen, H., 2007. Wintertime warming of an Arctic shelf in response to large-scale atmospheric circulation. Geophys. Res. Lett. 34, L10607. https://doi.org/10.1029/2007GL029948.

Cowan, E., Powell, R., 1991. Ice-proximal sediment accumulation rates in a temperate glacial fjord, southeastern Alaska. Glacial Mar. Sediment. Paleoclimatic Significance 261, 61.

Cowton, T.R., Sole, A.J., Nienow, P.W., Slater, D.A., Christoffersen, P., 2018. Linear response of east Greenland's tidewater glaciers to ocean/atmosphere warming. Proc. Natl. Acad. Sci. 115, 7907–7912. https://doi.org/10.1073/pnas.1801769115.

Grebmeier, J.M., 2012. Shifting patterns of life in the pacific arctic and sub-arctic seas. Ann. Rev. Mar. Sci. 4, 63–78. https://doi.org/10.1146/annurev-marine-120710-100926.

Hegseth, E.N., Sundfjord, A., 2008. Intrusion and blooming of Atlantic phytoplankton species in the high Arctic. J. Mar. Syst. 74, 108–119. https://doi.org/10.1016/j.jmarsys.2007.11.011.

Hegseth, E.N., Tverberg, V., 2013. Effect of Atlantic water inflow on timing of the phytoplankton spring bloom in a high Arctic fjord (Kongsfjorden, Svalbard). J. Mar. Syst. 113–114, 94–105. https://doi.org/10.1016/j.jmarsys.2013.01.003.

Helbling, E.W., Eilertsen, H.C., Villafañe, V.E., Holm-Hansen, O., 1996. Effects of UV radiation on post-bloom phytoplankton populations in Kvalsund, North Norway. J. Photochem. Photobiol. B Biol. 33, 255–259. https://doi.org/10.1016/1011-1344(95)07261-6.

Holland, D.M., Thomas, R.H., De Young, B., Ribergaard, M.H., Lyberth, B., 2008. Acceleration of Jakobshavn Isbrae triggered by warm subsurface ocean waters. Nat. Geosci. 1, 659–664. https://doi.org/10.1038/ngeo316.

Hop, H., Falk-Petersen, S., Svendsen, H., Kwasniewski, S., Pavlov, V., Pavlova, O., Søreide, J.E., 2006. Physical and biological characteristics of the pelagic system across Fram Strait to Kongsfjorden. Prog. Oceanogr. 71, 182–231. https://doi.org/10.1016/j.pocean.2006.09.007.

Hop, H., Pearson, T., Hegseth, E.N., Kovacs, K.M., Wiencke, C., Kwasniewski, S., Eiane, K., Mehlum, F., Gulliksen, B., Wlodarska-Kowalczuk, M., Lydersen, C., Weslawski, J.M., Cochrane, S., Gabrielsen, G.W., Leakey, R.J.G., Lønne, O.J., Zajaczkowski, M., Falk-Petersen, S., Kendall, M., Wängberg, S.-Å., Bischof, K., Voronkov, A.Y., Kovaltchouk, N.A., Wiktor, J., Poltermann, M., Prisco, G. di, Papucci, C., Gerland, S., 2002. The marine ecosystem of Kongsfjorden, Svalbard. Polar Res. 21, 167–208. https://doi.org/10.3402/polar.v21i1.6480.

Hopkins, T.S., 1991. The GIN Sea-A synthesis of its physical oceanography and literature review 1972-1985. Earth Sci. Rev. 30, 175–318. https://doi.org/10.1016/0012-8252(91)90001-V.

Hopwood, M.J., Carroll, D., Browning, T.J., Meire, L., Mortensen, J., Krisch, S., Achterberg, E.P., 2018. Non-linear response of summertime marine productivity to increased meltwater discharge around Greenland. Nat. Commun. 9 https://doi.org/10.1038/s41467-018-05488-8.

Jenkins, A., 2011. Convection-driven melting near the grounding lines of ice shelves and tidewater glaciers. J. Phys. Oceanogr. 41, 2279–2294. https://doi.org/10.1175/JPO-D-11-03.1.

Joughin, I., Smith, B.E., Shean, D.E., Floricioiu, D., 2014. Brief communication: further summer speedup of jakobshavn isbræ. Cryosphere 8, 209–214. https://doi.org/10.5194/tc-8-209-2014.

Juul-Pedersen, T., Arendt, K.E., Mortensen, J., Blicher, M.E., Søgaard, D.H., Rysgaard, S., 2015. Seasonal and interannual phytoplankton production in a sub-Arctic tidewater outlet glacier fjord, SW Greenland. Mar. Ecol. Prog. Ser. 524, 27–38. https://doi.org/10.3354/meps11174.

Kattsov, V., Källén, E., Cattle, H., Christensen, J., Drange, H., Hanssen-Bauer, I., Jóhannesen, T., Karol, I., Räisänen, J., Svensson, G., Vavulin, S., 2005. Future Climate Change: Modeling and Scenarios for the Arctic.

Kirk, J.T.O., 1994. Light and Photosynthesis in Aquatic Ecosystems. Cambridge university press.

Kwok, R., 2018. Arctic sea ice thickness, volume, and multiyear ice coverage: losses and coupled variability (1958-2018). Environ. Res. Lett. 13, 105005. https://doi.org/10.1088/1748-9326/aae3ec.

Laxon, S.W., Giles, K.A., Ridout, A.L., Wingham, D.J., Willatt, R., Cullen, R., Kwok, R., Schweiger, A., Zhang, J., Haas, C., Hendricks, S., Krishfield, R., Kurtz, N., Farrell, S., Davidson, M., 2013. CryoSat-2 estimates of Arctic sea ice thickness and volume. Geophys. Res. Lett. 40, 732–737. https://doi.org/10.1002/grl.50193.

Lefauconnier, B., Hagen, J.O., Rudant, J.P., 1994. Flow speed and calving rate of Kongsbreen glacier, Svalbard, using SPOT images. Polar Res. 13, 59–65. https://doi.org/10.1111/j.1751-8369.1994.tb00437.x.

Li, W.K.W., McLaughlin, F.A., Lovejoy, C., Carmack, E.C., 2009. Smallest algae thrive as the Arctic Ocean freshens. Science 326, 539. https://doi.org/10.1126/science.1179798 (80-.).

Luckman, A., Benn, D.I., Cottier, F., Bevan, S., Nilsen, F., Inall, M., 2015. Calving rates at tidewater glaciers vary strongly with ocean temperature. Nat. Commun. 6, 1–7. https://doi.org/10.1038/ncomms9566.

Meire, L., Mortensen, J., Meire, P., Juul-Pedersen, T., Sejr, M.K., Rysgaard, S., Nygaard, R., Huybrechts, P., Meysman, F.J.R., 2017. Marine-terminating glaciers sustain high productivity in Greenland fjords. Glob. Chang. Biol. 23, 5344–5357. https://doi.org/10.1111/gcb.13801.

Meire, L., Mortensen, J., Rysgaard, S., Bendtsen, J., Boone, W., Meire, P., Meysman, F.J.R., 2016. Spring bloom dynamics in a subarctic fjord influenced by tidewater outlet glaciers (Godthåbsfjord, SW Greenland). J. Geophys. Res. Biogeosci. 1581–1592. https://doi.org/10.1002/2015JG003240.Received.

Morel, F., Morgan, J., 1972. A numerical method for computing equilibria in aqueous chemical systems. Environ. Sci. Technol. 6, 58–67. https://doi.org/10.1021/es60060a006.

Mortenson, E., Steiner, N., Monahan, A.H., Miller, L.A., Geilfus, N.-X., Brown, K., 2018. A model-based analysis of physical and biogeochemical controls on carbon exchange in the upper water column, sea ice, and atmosphere in a seasonally ice-covered Arctic strait. J. Geophys. Res. Ocean. https://doi.org/10.1029/2018JC014376.

Motyka, R.J., Dryer, W.P., Amundson, J., Truffer, M., Fahnestock, M., 2013. Rapid submarine melting driven by subglacial discharge, LeConte Glacier, Alaska. Geophys. Res. Lett. 40, 5153–5158. https://doi.org/10.1002/grl.51011.

Murray, A.T., Scharrer, K., Selmes, N., Booth, A.D., James, T.D., Bevan, S., Bradley, J., Cook, S., Cordero-Llana, L., Drocourt, Y., Dyke, L., Goldsack, A., Hughes, A., Luckman, A., McGovern, J., 2015. Extensive retreat of Greenland tidewater glaciers. Arctic Antarct. Alpine Res. 47, 427–447. https://doi.org/10.1657/AAAR0014-049.

Neale, P.J., Davis, R.F., Cullen, J.J., 1998. Interactive effects of ozone depletion and vertical mixing on photosynthesis of Antartic phytoplankton. Nature 392, 585–589.

Neukermans, G., Oziel, L., Babin, M., 2018. Increased intrusion of warming Atlantic water leads to rapid expansion of temperate phytoplankton in the Arctic. Glob. Chang. Biol. 24, 2545–2553. https://doi.org/10.1111/gcb.14075.

Nilsen, F., Skogseth, R., Vaardal-Lunde, J., Inall, M., 2016. A simple shelf circulation model: intrusion of atlantic water on the west spitsbergen shelf. J. Phys. Oceanogr. 46, 1209–1230. https://doi.org/10.1175/JPO-D-15-0058.1.

Onarheim, I.H., Smedsrud, L.H., Ingvaldsen, R.B., Nilsen, F., 2014. Loss of sea ice during winter north of Svalbard. Tellus Ser. A Dyn. Meteorol. Oceanogr. 66, 23933. https://doi.org/10.3402/tellusa.v66.23933.

Osborne, E., Richter-Menge, J., Jeffries, M., 2018. Arctic Report Card 2018.

Overland, J.E., Hanna, E., Hanssen-Bauer, I., Kim, S.-J., Walsh, J.E., Wang, M., Bhatt, U. S., Thoman, R.L., 2017. Surface air temperature. Arct. Rep. Card, 2017.

Pavlov, A.K., Silyakova, A., Granskog, M.A., Bellerby, R.G.J., Engel, A., Schulz, K.G., Brussaard, C.P.D., 2014. Marine CDOM accumulation during a coastal Arctic mesocosm experiment: No response to elevated pCO2 levels. J. Geophys. Res. 119, 1216–1230. https://doi.org/10.1002/2013JG002588.Received.

Pavlov, A.K., Tverberg, V., Ivanov, B.V., Nilsen, F., Falk-Petersen, S., Granskog, M.A., 2013. Warming of Atlantic water in two west Spitsbergen fjords over the last century (1912-2009). Polar Res. 32, 11206. https://doi.org/10.3402/polar.v32i0.11206.

Perovich, D.K., 2018. Sunlight, clouds, sea ice, albedo, and the radiative budget : the umbrella versus the blanket. Cryosphere 12, 2159–2165.

Pithan, F., Mauritsen, T., 2014. Arctic amplification dominated by temperature feedbacks in contemporary climate models. Nat. Geosci. 7, 181–184. https://doi.org/10.1038/ngeo2071.

Polyakov, I.V., Alexeev, V.A., Ashik, I.M., Bacon, S., Beszczynska-Möller, A., Carmack, E. C., Dmitrenko, I.A., Fortier, L., Gascard, J.C., Hansen, E., Hölemann, J., Ivanov, V.V., Kikuchi, T., Kirillov, S., Lenn, Y.D., McLaughlin, F.A., Piechura, J., Repina, I., Timokhov, L.A., Walczowski, W., Woodgate, R., 2011. Fate of early 2000s arctic warm water pulse. Bull. Am. Meteorol. Soc. 92, 561–566. https://doi.org/10.1175/2010BAMS2921.1.

Polyakov, I.V., Beszczynska, A., Carmack, E.C., Dmitrenko, I.A., Fahrbach, E., Frolov, I. E., Gerdes, R., Hansen, E., Holfort, J., Ivanov, V.V., Johnson, M.A., Karcher, M., Kauker, F., Morison, J., Orvik, K.A., Schauer, U., Simmons, H.L., Skagseth, O., Sokolov, V.T., Steele, M., Timokhov, L.A., Walsh, D., Walsh, J.E., 2005. One more step toward a warmer Arctic. Geophys. Res. Lett. 32, L17605. https://doi.org/10.1029/2005GL023740.

Polyakov, I.V., Pnyushkov, A.V., Timokhov, L.A., 2012. Warming of the intermediate Atlantic water of the Arctic ocean in the 2000s. J. Clim. 25, 8362–8370. https://doi.org/10.1175/JCLI-D-12-00266.1.

Post, E., Forchhammer, M., Bret-Harte, M., Callaghan, T., Christensen, T., Elberling, B., Fox, A., Gilg, O., Hik, D., Høye, T., Ims, R., Jeppesen, E., Klein, D., Madsen, J., Aastrup, P., 2009. Ecological dynamics across the arctic associated with recent climate change. Science 325, 1355–1359. https://doi.org/10.1126/science.1173113 (80-.).

Rajagopalan, D., 2012. Characterizing fjord oceanography near tidewater glaciers Kronebreen and Kongsvegen. In: Kongsfjorden, Svalbard. Yale, College.

Rignot, E., Koppes, M., Velicogna, I., 2010. Rapid submarine melting of the calving faces of West Greenland glaciers. Nat. Geosci. 3, 187–191. https://doi.org/10.1038/ngeo765.

Roesler, C.S., Barnard, A.H., 2013. Optical proxy for phytoplankton biomass in the absence of photophysiology: rethinking the absorption line height. Methods Oceanogr. 7, 79–94. https://doi.org/10.1016/j.mio.2013.12.003.

Sallee, J.-B., 2018. Southern ocean warming. Oceanography 31, 52–62. https://doi.org/10.5670/oceanog.2009.80 (COPYRIGHT).

Schellenberger, T., Dunse, T., Kääb, A., Kohler, J., Reijmer, C.H., 2015. Surface speed and frontal ablation of Kronebreen and Kongsbreen, NW Svalbard, from SAR offset tracking. Cryosphere 9, 2339–2355. https://doi.org/10.5194/tc-9-2339-2015.

Screen, J.A., Simmonds, I., 2010. The central role of diminishing sea ice in recent Arctic temperature amplification. Nature 464, 1334–1337. https://doi.org/10.1038/nature09051.

Serreze, M.C., Stroeve, J., 2015. Arctic sea ice trends, variability and implications for seasonal ice forecasting. Philos. Trans. R. Soc. Lond. 20140159.

Slater, D.A., Straneo, F., Das, S.B., Richards, C.G., Wagner, T.J.W., Nienow, P.W., 2018. Localized plumes drive front-wide ocean melting of A Greenlandic Tidewater Glacier. Geophys. Res. Lett. 45 (12) https://doi.org/10.1029/2018GL080763, 350-12,358.

Smith, R.C., Baker, K.S., 1981. Optical properties of the clearest natural waters (200–800 nm). Appl. Opt. 20, 177–184. https://doi.org/10.1364/AO.20.000177.

Spielhagen, R.F., Werner, K., Sørensen, S.A., Zamelczyk, K., Kandiano, E., Budeus, G., Husum, K., Marchitto, T.M., Hald, M., 2011. Enhanced modern heat transfer to the arctic by warm atlantic water. Science 331, 450–453 (80-.).

Stramski, D., Babin, M., Wozniak, S.B., 2007. Variations in the optical properties of terrigenous mineral-rich particulate matter suspended in seawater. Limnol. Oceanogr. 52, 2418–2433. https://doi.org/10.4319/lo.2007.52.6.2418.

Straneo, F., Cenedese, C., 2015. The dynamics of Greenland's glacial fjords and their role in climate. Ann. Rev. Mar. Sci. 7, 89–112. https://doi.org/10.1146/annurev-marine-010213-135133.

Straneo, F., Heimbach, P., 2013. North Atlantic warming and the retreat of Greenland's outlet glaciers. Nature 504, 36–43. https://doi.org/10.1038/nature12854.

Stroeve, J.C., Kattsov, V., Barrett, A., Serreze, M., Pavlova, T., Holland, M., Meier, W.N., 2012. Trends in Arctic sea ice extent from CMIP5, CMIP3 and observations. Geophys. Res. Lett. 39, L16502. https://doi.org/10.1029/2012GL052676.

Sund, M., Eiken, T., Rolstad Denby, C., 2011. Velocity structure, front position changes and calving of the tidewater glacier Kronebreen, Svalbard. Cryosphere Discuss. 5, 41–73. https://doi.org/10.5194/tcd-5-41-2011.

Svendsen, H., Beszczynska-Møller, A., Hagen, J.O., Lefauconnier, B., Tverberg, V., Gerland, S., Ørbæk, J.B., Bischof, K., Papucci, C., Zajaczkowski, M., Azzolini, R., Bruland, O., Wiencke, C., Winther, J.-G., Dallmann, W., 2002. The physical environment of Kongsfjorden–Krossfjorden, an Arctic fjord system in Svalbard. Polar Res. 21, 133–166. https://doi.org/10.1111/j.1751-8369.2002.tb00072.x.

Truffer, M., Motyka, R.J., 2016. Where glaciers meet water: subaqueous melt and its relevance to glaciers in various settings. Rev. Geophys. 54, 220–239. https://doi.org/10.1002/2015RG000494.

Trusel, L.D., Powell, R.D., Cumpston, R.M., Brigham-Grette, J., 2010. Modern glacimarine processes and potential future behaviour of Kronebreen and Kongsvegen polythermal tidewater glaciers, Kongsfjorden, Svalbard. Fjord Syst. Arch. Geol. Soc. London, Spec. Publ. 344, 89–102. https://doi.org/10.1144/SP344.9.

Twardowski, M.S., Boss, E., Macdonald, J.B., Pegau, W.S., Barnard, A.H., Zaneveld, J.R. V., 2001. A model for estimating bulk refractive index from the optical backscattering ratio and the implications for understanding particle composition in case I and case II waters. J. Geophys. Res. Ocean 106, 14129–14142. https://doi.org/10.1029/2000JC000404.

Vallot, D., Pettersson, R., Luckman, A., Benn, D.I., Zwinger, T., Van Pelt, W.J.J., Kohler, J., Schäfer, M., Claremar, B., Hulton, N.R.J., 2017. Basal dynamics of Kronebreen, a fast-flowing tidewater glacier in Svalbard: non-local spatio-Temporal response to water input. J. Glaciol. 63, 1012–1024. https://doi.org/10.1017/jog.2017.69.

Vinje, T., 2001. Anomalies and trends of sea-ice extent and atmospheric circulation in the Nordic Seas during the period 1864-1998. J. Clim. 14, 255–267. https://doi.org/10.1175/1520-0442(2001)014<0255:AATOSI>2.0.CO;2.

Walczowski, W., Piechura, J., 2007. Pathways of the Greenland sea warming. Geophys. Res. Lett. 34, L10608. https://doi.org/10.1029/2007GL029974.

Wassmann, P., 2011. Arctic marine ecosystems in an era of rapid climate change. Prog. Oceanogr. 90, 1–17. https://doi.org/10.1016/j.pocean.2011.02.002.

Willis, K.J., Cottier, F.R., Kwaśniewski, S., 2008. Impact of warm water advection on the winter zooplankton community in an Arctic fjord. Polar Biol. 31, 475–481. https://doi.org/10.1007/s00300-007-0373-0.